

# Particle acceleration and synchrotron emission in blazar jets

J.G. Kirk<sup>1</sup>, F.M. Rieger<sup>2</sup>, and A. Mastichiadis<sup>3</sup>

<sup>1</sup> Max-Planck-Institut für Kernphysik, Postfach 10 39 80, D-69029 Heidelberg, Germany

<sup>2</sup> Universitätssternwarte, Geismarlandstrasse 11, D-37083 Göttingen, Germany

<sup>3</sup> University of Athens, Department of Physics, Panepistimiopolis, GR-157 83 Zografos, Greece

Received 13 October 1997 / Accepted 27 January 1998

**Abstract.** We model the acceleration of electrons at a shock front in a relativistic blazar jet and compute the radiation they emit in a post-shock region which contains a homogeneous magnetic field. The full space, time and momentum dependence of the electron distribution is used in this calculation. It is shown that the ‘homogeneous’ synchrotron model is recovered, provided the downstream speed of the plasma away from the shock front is nonrelativistic, and provided that the light travel times across the face of the shock front is unimportant. By varying the rate at which particles are picked up by the acceleration process, we calculate the time-dependence of the spectra. Since the magnetic field strength is assumed constant within the emission region, each frequency band can be identified with electrons of a particular energy. We find that for a band in which the electrons are accelerated rapidly compared to the rate at which they cool, the spectra typically harden during phases of rising flux, and soften during phases of falling flux, as has been observed in the objects PKS 2155–304 and Mkn 421. However, in a frequency band in which the timescales are comparable, the reverse behaviour is to be expected. We discuss the extent to which observations of both the stationary spectrum and the spectral variability of the synchrotron component of blazar emission can be used to constrain the model.

**Key words:** acceleration of particles – radiation mechanisms: non-thermal – shock waves – galaxies: jets

## 1. Introduction

The nonthermal, highly variable X-ray emission of blazars is usually interpreted as the synchrotron emission of relativistic electrons accelerated in a jet which itself moves at relativistic speed towards the observer. In this scenario, the higher energy gamma-rays detected from several such sources arise from the inverse Compton scattering of soft photons by these electrons (for a review, see Sikora 1994). Two different types of model of the emitting region can be found in the literature: the ‘inhomogeneous’ and the ‘homogeneous’ models. In the inhomogeneous model, the emitting part of the jet is assumed to be cylindrically

symmetric with a cross-section which varies with distance from the central object. The magnetic field is also taken to vary with distance from the central object. It is usually assumed that relativistic electrons are ‘injected’ at a shock front which moves through the emission region, starting close to the central object. These electrons also move outwards with the jet material, and undergo energy losses due both to synchrotron radiation and to the adiabatic expansion of the jet (Marscher & Gear 1996, Maraschi, Ghisellini & Celotti 1992, Marscher & Travis 1996). The resulting synchrotron spectrum is found by integrating over the emission region, within which both the magnetic field and the particle distribution is inhomogeneous.

In the homogeneous model, on the other hand, both the magnetic field and the particle distribution function are assumed homogeneous throughout the emission region (Inoue & Takahara 1996, Chiaberge & Ghisellini 1997, Mastichiadis & Kirk 1997). The relativistic electrons are injected with a specified distribution and are assumed to escape on a timescale  $t_{\text{esc}}$ . After escape, a particle no longer radiates. Although at first sight somewhat arbitrary, there is a good observational reason to believe that escape, or, equivalently, sudden energy loss by adiabatic expansion, is important: the spectral index of the radio emission of blazars is typically hard ( $\alpha > -0.5$ ) and cannot be produced by particles which have been allowed to cool completely by synchrotron emission. If we adopt a strictly homogeneous model, electrons must escape from the emission region and thus be prevented from cooling completely. Such a picture departs from the standard explanation, in which the flat spectrum is thought to be the result of a variation of the self-absorption frequency within the source in an inhomogeneous model (the ‘Cosmic Conspiracy’ Marscher 1980). Depending on the magnetic field strength and Doppler boosting factor, self-absorption may also become important in a homogeneous model. Additional components emitting at low frequency would then be required.

The homogeneous model with escape corresponds approximately to the plausible physical situation in which particles are accelerated at a shock front, provided there is a region of relatively high magnetic field just behind the shock. In this case, radiation from this region may be expected to dominate the observed emission. This requires that on leaving the region (on a timescale  $t_{\text{esc}}$ ), the particles encounter a magnetic field that is

so weak, that no significant further contribution to the emitted spectrum arises, despite the fact that particles accumulate there over the entire life of the source. However, a problem arises in the homogeneous model concerning time variability – only if the physical dimensions of the source are such that the light crossing time is short compared with the synchrotron cooling time is it reasonable to assume homogeneity. If this condition is not fulfilled, the observed variability is dominated by the shape and orientation of the source, rather than the intrinsic cooling and acceleration timescales. Until recently, models of the rapid variability of blazars have either fulfilled this condition or have made specific assumptions about the source geometry (Mastichiadis & Kirk 1997, Chiaberge & Ghisellini 1997).

In this paper we present a model in which particles are accelerated at a shock front and cool by synchrotron radiation in the homogeneous magnetic field behind it. The plasma downstream of the shock front moves relativistically towards the observer; the shock front is nonrelativistic when seen from the rest frame of the downstream plasma. The kinetic equations are solved for the time, space and energy dependences of the particle distribution function, and the resulting synchrotron emission is calculated. ‘Escape’ is accounted for by assuming that the magnetic field strength drops suddenly at a finite distance behind the shock, so that the radiation from the adiabatically cooled electrons in the weaker field can be neglected. Thus, this model is homogeneous in the sense that the magnetic field does not vary through the emission region, but contains an inhomogeneous electron distribution. The variability is computed by assuming the observer lies in the direction of the normal to the shock front. This preferred orientation does not affect the observed variability provided the light travel time across the face of the source (i.e., over the surface of the shock) is short compared to the synchrotron cooling time as measured in the rest frame of the plasma. At the highest electron energies considered in the application to X-ray blazars, this condition may be violated, in which case the computed variability will be smoothed out over the longer timescale. Whether or not this is expected to occur could be decided by comparing the predicted emission by inverse Compton scattering with gamma-ray observations. In principle, observations of the frequency dependence of the variation timescale could also resolve the question.

We consider only the synchrotron radiation of the accelerated particles, leaving the more involved computation of the inverse Compton emission to future work. This is sufficient for comparison with the observed radio to X-ray emission of blazars, provided the energy losses of the electrons are not dominated by inverse Compton scattering, which is usually the case, at least for BL Lac-type objects (Comastri et al. 1997).

## 2. The electron distribution function

Consider, then a shock front propagating along a cylindrical jet of constant cross-section. Electrons are accelerated at the shock front, and subsequently drift away from it in the downstream flow. Following Ball & Kirk (1992), we treat two spatial zones: one around the shock front, in which particles are continuously

accelerated, and one downstream of it, in which particles emit most of the radiation. In each zone, it is assumed that pitch-angle scattering maintains an almost isotropic particle distribution. The number  $N(\gamma)d\gamma$  of particles with Lorentz factor between  $\gamma$  and  $\gamma+d\gamma$  in the acceleration zone around the shock is governed by the equation

$$\frac{\partial N}{\partial t} + \frac{\partial}{\partial \gamma} \left[ \left( \frac{\gamma}{t_{\text{acc}}} - \beta_s \gamma^2 \right) N \right] + \frac{N}{t_{\text{esc}}} = Q\delta(\gamma - \gamma_0) \quad (1)$$

(Kirk et al. 1994), where

$$\beta_s = \frac{4}{3} \frac{\sigma_T}{m_e c} \left( \frac{B^2}{2\mu_0} \right). \quad (2)$$

with  $\sigma_T = 6.65 \cdot 10^{-29} \text{m}^2$  the Thomson cross section. The first term in brackets in Eq. (1) describes acceleration at the rate  $t_{\text{acc}}^{-1}$ , the second describes the rate of energy loss due to synchrotron radiation averaged over pitch-angle (because of the isotropy of the distribution) in a magnetic field  $B$  (in Tesla). Particles are assumed to escape from this region at an energy independent rate  $t_{\text{esc}}^{-1}$ , and to be picked up (injected) into the acceleration process with Lorentz factor  $\gamma_0$  at a rate  $Q$  particles per second. Note that the concept of this ‘acceleration zone’ differs from the emission region in the usual homogeneous models in two important respects: a) particles are injected at low energy and continuously accelerated and b) very little radiation is emitted by a particle whilst in the acceleration zone (see the discussion below).

Assuming a constant injection rate  $Q_0$  after switch-on at time  $t = 0$ , and setting  $N(\gamma) = 0$  for  $t \leq 0$ , Eq. (1) has the solution

$$N(\gamma, t) = a \frac{1}{\gamma^2} \left( \frac{1}{\gamma} - \frac{1}{\gamma_{\text{max}}} \right)^{(t_{\text{acc}} - t_{\text{esc}})/t_{\text{esc}}} \times \Theta(\gamma - \gamma_0) \Theta(\gamma_1(t) - \gamma), \quad (3)$$

for  $\gamma_0 < \gamma < \gamma_1(t)$ , and  $N(\gamma, t) = 0$ , otherwise. Here  $\Theta(x)$  is the Heaviside step function,

$$a = Q_0 t_{\text{acc}} \gamma_0^{t_{\text{acc}}/t_{\text{esc}}} \left( 1 - \frac{\gamma_0}{\gamma_{\text{max}}} \right)^{-t_{\text{acc}}/t_{\text{esc}}}, \quad (4)$$

and the upper bound  $\gamma_1(t)$  is determined by

$$\gamma_1(t) = \left( \frac{1}{\gamma_{\text{max}}} + \left[ \frac{1}{\gamma_0} - \frac{1}{\gamma_{\text{max}}} \right] e^{-t/t_{\text{acc}}} \right)^{-1}, \quad (5)$$

with  $\gamma_{\text{max}} = (\beta_s t_{\text{acc}})^{-1}$ . The quantities  $t_{\text{acc}}$  and  $t_{\text{esc}}$  have been assumed independent of energy in this solution, the more general solution allowing for energy dependence is given in the Appendix.

In the model developed by Ball & Kirk (1992), accelerated particles escape into the downstream plasma, where they radiate. We can formulate the kinetic equation obeyed by the density of particles in the radiation zone most compactly using a coordinate system at rest in the radiating plasma. The shock front then provides a moving source of electrons, which subsequently suffer energy losses, but are assumed not to be transported in

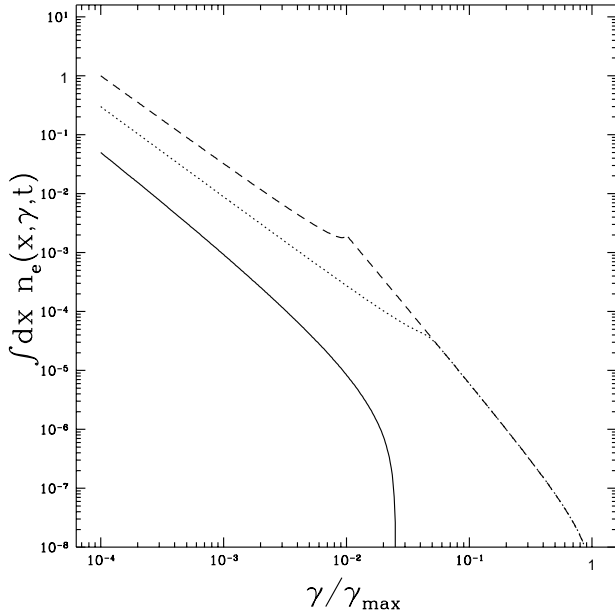


**Fig. 1.** The electron distribution integrated over the source, as given by Eq. (10). The three curves correspond to the times  $5t_{\text{acc}}$  (solid line),  $30t_{\text{acc}}$  (dotted line) and  $500t_{\text{acc}}$  (dashed line). At larger times the distribution does not evolve appreciably. For this plot,  $t_{\text{esc}} = 2t_{\text{acc}}$  (i.e.,  $s = 3.5$ ) and  $t_b = 100t_{\text{acc}}$ . At  $t = 5t_{\text{acc}}$ , no particles have had time to cool, since the cooling time at the maximum Lorentz factor of  $\gamma \approx 0.025\gamma_{\text{max}}$  is approximately  $40t_{\text{acc}}$ . At times  $t > 500t_{\text{acc}}$  all particles with  $\gamma > \gamma_{\text{max}}t_{\text{acc}}/t_b$  cool, whereas those of lower  $\gamma$  leave the source without significant loss of energy.

space. The kinetic equation governing the differential density  $dn(x, \gamma, t)$  of particles in the range  $dx, d\gamma$  is then

$$\frac{\partial n}{\partial t} - \frac{\partial}{\partial \gamma} (\beta_s \gamma^2 n) = \frac{N(\gamma, t)}{t_{\text{esc}}} \delta(x - x_s(t)) \quad (6)$$

where  $x_s(t)$  is the position of the shock front at time  $t$ . For a shock which starts to accelerate (and therefore ‘inject’) particles at time  $t = 0$  and position  $x = 0$  and moves at constant speed  $u_s$ , the solution of Eq. (6) for  $\gamma > \gamma_0$  is

$$n(x, \gamma, t) = \frac{a}{u_s t_{\text{esc}} \gamma^2} \left[ \frac{1}{\gamma} - \beta_s \left( t - \frac{x}{u_s} \right) - \frac{1}{\gamma_{\text{max}}} \right]^{(t_{\text{acc}} - t_{\text{esc}})/t_{\text{esc}}} \Theta \left[ \gamma_1(x/u_s) - (1/\gamma - \beta_s t + \beta_s x/u_s)^{-1} \right], \quad (7)$$

where  $\gamma_1(t)$  is given by Eq. (5). To obtain the synchrotron emissivity as a function of position, time and frequency we convolve the density  $n$  with the synchrotron Green’s function  $P(\nu, \gamma)$ . A convenient approximation to this function is given by Melrose (1980):

$$P(\nu, \gamma) = a_s z^{0.3} \exp(-z) \quad (8)$$

where  $a_s = \sqrt{3}e^2 \Omega \sin \theta / (2\pi c)$  is a constant and  $z \equiv 4\pi\nu / (3\Omega \sin \theta \gamma^2)$ , with  $\Omega = eB/m$  the electron gyro frequency and  $\theta$  the angle between the magnetic field direction

and the line of sight. At a point  $x = X (> u_s t)$  on the symmetry axis of the source at time  $t$  the specific intensity of radiation in the  $x$  direction depends on the retarded time  $\bar{t} = t - X/c$  and is given by

$$I_0(\nu, \bar{t}) = \int d\gamma P(\nu, \gamma) \int dx n(x, \gamma, \bar{t} + x/c) \quad (9)$$

and the integrated particle density can readily be evaluated:

$$\int dx n(x, \gamma, \bar{t} + x/c) = \frac{a}{(1 - u_s/c) \gamma_{\text{max}}^{(t_{\text{acc}} + t_{\text{esc}})/t_{\text{esc}}}} \left( \frac{\gamma_{\text{max}}}{\gamma} \right)^2 \left\{ \left[ \frac{\gamma_{\text{max}}}{\gamma} - \frac{\bar{t}}{t_{\text{acc}}} + \frac{x(1 - u_s/c)}{u_s t_{\text{acc}}} - 1 \right]^{t_{\text{acc}}/t_{\text{esc}}} \right\}_{x_0(\gamma, \bar{t})}^{x_1(\bar{t})}. \quad (10)$$

The limits of the spatial integration are given by the retarded position of the shock front

$$x_1(\bar{t}) = \frac{u_s \bar{t}}{1 - (u_s/c)}. \quad (11)$$

and the retarded position  $x_0(\gamma, \bar{t})$  of the point furthest from the shock front at which particles have Lorentz factor  $\gamma$  at time  $\bar{t} + x_0/c$ . This is given either by the solution  $x_{\text{cool}}(\gamma, \bar{t})$  of the transcendental equation

$$\left[ \frac{\gamma_{\text{max}}}{\gamma} - \frac{\bar{t} + x_{\text{cool}}/c}{t_{\text{acc}}} + \frac{x_{\text{cool}}}{u_s t_{\text{acc}}} \right] = 1 + \left( \frac{\gamma_{\text{max}}}{\gamma_0} - 1 \right) \exp[-x_{\text{cool}}/(u_s t_{\text{acc}})] \quad (12)$$

or by the assumed maximum spatial extent of the emission region (i.e., the point at which the magnetic field declines substantially). Denoting this distance by  $L$ , we have

$$x_0(\gamma, \bar{t}) = \text{Max} [x_{\text{cool}}(\gamma, \bar{t}), x_1(\bar{t}) - L] \quad (13)$$

This is most conveniently expressed in terms of the (retarded) time  $t_b$  for the plasma to traverse the emitting region, as measured in the plasma rest frame:

$$t_b = \frac{(1 - u_s/c)L}{u_s} \quad (14)$$

Eq. (10) gives the integrated particle density for times greater than the ‘switch-on’ time:

$$\bar{t} > t_{\text{on}} = t_{\text{acc}} \left( 1 - \frac{u_s}{c} \right) \log \left[ \frac{(\gamma_{\text{max}}/\gamma_0) - 1}{(\gamma_{\text{max}}/\gamma) - 1} \right] \quad (15)$$

before which it vanishes. The resulting electron spectrum, integrated over the source is depicted in Fig. 1. A characteristic break in the spectral slope appears at a particular Lorentz factor  $\gamma_{\text{br}}(t)$  which, at any given time, separates those electrons which cool within the source ( $\gamma > \gamma_{\text{break}}$ ) from those which do not cool within the source ( $\gamma < \gamma_{\text{break}}$ ). At large times, all electrons with  $\gamma < \gamma_{\text{break}}(\infty) = \gamma_{\text{max}}/(1 + t_b/t_{\text{acc}})$  leave

the source before cooling, and the integrated electron density becomes time-independent.

A question which remains open in this approach is the synchrotron radiation emitted by a particle whilst in the acceleration region. If the magnetic field ahead of the shock were the same as that behind the shock, the total emission could easily be computed using Eq. (3). For  $t > t_{\text{on}}$ , we would have an extra contribution to the flux:

$$\begin{aligned} I_s(\nu, \bar{t}) &= \int d\gamma P(\nu, \gamma) \int dx N(\gamma, \bar{t}) \delta[x - u_s(\bar{t} + x/c)] \\ &= \frac{a}{(1 - u_s/c) \gamma_{\text{max}}^{(t_{\text{acc}} + t_{\text{esc}})/t_{\text{esc}}} \int d\gamma P(\nu, \gamma) \left( \frac{\gamma_{\text{max}}}{\gamma} \right)^2 \\ &\quad \left( \frac{\gamma_{\text{max}}}{\gamma} - 1 \right)^{(t_{\text{acc}} - t_{\text{esc}})/t_{\text{esc}}} \end{aligned} \quad (16)$$

and the total emission  $I_1(\nu, \bar{t})$  would be given by

$$I_1(\nu, \bar{t}) = I_0(\nu, \bar{t}) + I_s(\nu, \bar{t}) \quad (17)$$

However, for oblique shocks, the magnetic field strength is expected to increase upon compression at the shock. Particles undergoing acceleration spend part of the time in the upstream and part in the downstream plasma, so that it is not clear how to evaluate their synchrotron emission, although Eq. (16) certainly gives an upper limit. At oblique shocks, reflection at the front itself is thought to be more important than diffusion in the downstream zone, (Kirk & Heavens 1989), so that accelerating particles spend all their time upstream. In this case, it seems reasonable to neglect the emission from the acceleration zone completely, which is the approach adopted here. An improved treatment of this point demands a full time-dependent solution of the diffusion advection equation, which requires considerable numerical effort (Fritz & Webb 1990).

All quantities calculated so far in this section refer to the frame in which the radiating plasma is at rest (the jet frame). For application to blazars, they must be transformed into the observer's frame. Assuming the observer to lie in the direction of motion of the plasma, and denoting the plasma bulk velocity by  $c\beta_b$ , the relevant transformations are

$$X = \Gamma_b(D - \beta_b c t_{\text{obs}}) \quad (18)$$

$$t = \Gamma_b(t_{\text{obs}} - \beta_b D/c) \quad (19)$$

$$\nu_{\text{obs}} = \Gamma_b(1 + \beta_b)\nu \approx 2\Gamma_b\nu \quad (20)$$

$$I_{\text{obs}}(\nu_{\text{obs}}, t_{\text{obs}}) = (\nu_{\text{obs}}/\nu)^3 I(\nu, \bar{t}) \approx 8\Gamma_b^3 I(\nu, \bar{t}) \quad (21)$$

where  $\Gamma_b (\gg 1)$  is the Lorentz factor of the approaching jet plasma and  $D$  the position of the detector with respect to the position of the shock at  $t = 0$ , as measured in the observer's reference frame.

Several simple qualitative results follow from these expressions. Close to the maximum emitted frequency, the timescale on which the intensity varies in the frame of the plasma is roughly the switch-on time  $\sim (1 - u_s/c)t_{\text{acc}}$ . According to Eqs. (18) and (19),  $\bar{t} = (1 + \beta_b)\Gamma_b(t_{\text{obs}} - D/c)$ . Thus, the observed timescale is shorter than the intrinsic  $t_{\text{acc}}$  by a factor  $\Gamma_b(1 + \beta_b)/(1 - u_s/c)$ . Doppler boosting of the flux, is independent of the shock speed, and is given simply by Eq. (21).

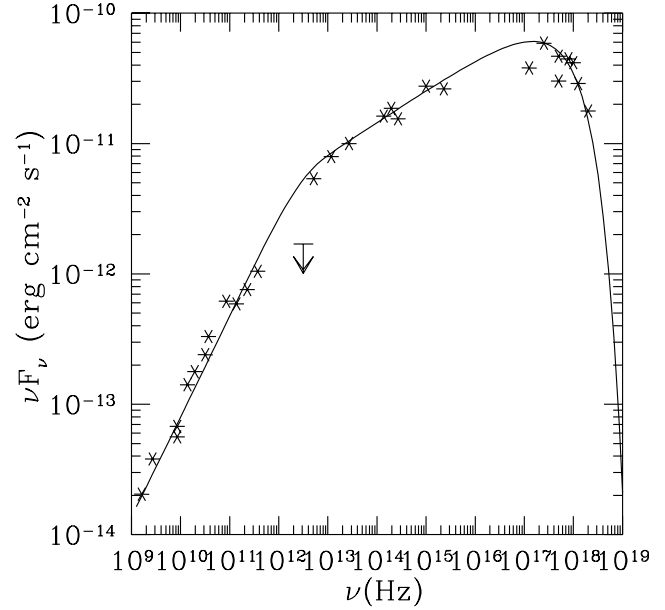


**Fig. 2.** The radio – X-ray spectrum of the object Mkn 501 (data taken from the collation of Catanese et al. 1997) together with the stationary synchrotron emission from a single homogeneous source

### 3. Application to the synchrotron spectra of blazars

The simple model described above provides a remarkably good fit to the radio to X-ray spectra of several blazars. As an example, we show in Fig. 2 observations of the object Mkn 501. The gamma-ray emission of this object, which has been the subject of much recent interest (e.g., Bradbury et al 1997), is not included in this figure, since it is not thought to arise as synchrotron radiation. For the X-ray emission we display the archival data selected by Catanese et al. (1997) and not the data taken during the TeV flare in April 1997.

The stationary emission ( $t \rightarrow \infty$ ) found from Eq. (9) by a single numerical quadrature over the synchrotron Green's function is also shown in Fig. 2. The form of the spectrum is very close to that given by Meisenheimer & Heavens (1987), who used an analytic solution to the stationary diffusion/advection equation, including synchrotron losses. Four free parameters are used to produce this fit:

1. the low frequency spectral index  $\alpha = -0.25$ , which corresponds to taking  $t_{\text{acc}} = t_{\text{esc}}/2$
2. the characteristic synchrotron frequency emitted by an electron of the maximum Lorentz factor as seen in the observers frame (taken to be  $1.3 \times 10^{18}$  Hz)
3. the spatial extent of the emitting region, which determines the position of the spectral break at roughly  $5 \times 10^{12}$  Hz, corresponding to  $t_b = 700t_{\text{acc}}$
4. the absolute flux level.

Since we restrict our model to the synchrotron emission of the accelerated particles, it is not possible independently to constrain quantities such as the Doppler boosting factor, or the magnetic field. These can, however, be found using a model for the gamma-ray emission, for example the synchrotron self-

compton model (Mastichiadis & Kirk 1997). Similarly, the frequency below which synchrotron self-absorption modifies the optically thin spectrum is not constrained within the current picture. Nevertheless, our model of the synchrotron emission makes predictions concerning the spectral variability in each of the three characteristic frequency ranges which can be identified in Fig. 2. These ranges are generic features of any synchrotron model, so that the predicted variability can easily be applied to the synchrotron emission of other blazars. They are a) the low frequency region, where the particles have not had time to cool before leaving the source (this is the region with  $\alpha = -0.25$  in Fig. 2, below the break at  $5 \times 10^{12}$  Hz) b) the region between the break and the maximum flux, where the particles have had time to cool, but where the cooling rate is always much slower than the acceleration rate and the spectrum is close to  $\alpha = -0.75$ , and c) the region around and above the flux maximum at roughly  $10^{17}$  Hz, where the acceleration rate is comparable to the cooling rate.

Variability or flaring behaviour can arise for a number of reasons. When the shock front overruns a region in the jet in which the local plasma density is enhanced, the number of particles picked up and injected into the acceleration process might be expected to increase. In addition, if the density change is associated with a change in the magnetic field strength, the acceleration timescale might also change, and, hence, the maximum frequency of the emitted synchrotron radiation. Considering the case in which the acceleration timescale remains constant, it is a simple matter to compute the emission, since Eq. (6) is linear. An increase of the injection rate by a factor  $1 + \eta_f$  for a time  $t_f$  is found by setting

$$Q(t) = Q_0 \quad \text{for } t < 0 \text{ and } t > t_f \quad (22)$$

$$Q(t) = (1 + \eta_f)Q_0 \quad \text{for } 0 < t < t_f \quad (23)$$

We then have

$$I(\nu, \bar{t}) = I_1(\nu, \infty) + \eta_f [I_1(\nu, \bar{t}) - I_1(\nu, \bar{t} - (1 - u_s/c)t_f)] \quad (24)$$

Using  $\eta_f = 1$ ,  $t_f = 10t_{\text{acc}}$  and  $u_s = c/10$ , we show the resulting emission at a frequency  $\nu = \nu_{\text{max}}/100$  in Fig. 3. In the case of Mkn 501, this corresponds to a frequency of about  $10^{16}$  Hz, which lies towards the high frequency part of region b), between the infra-red and X-ray regions, where the spectral index is close to  $\alpha = -0.75$ . Also shown in this figure is the temporal behaviour of the spectral index, as determined from the ratio of the fluxes at  $0.01\nu_{\text{max}}$  and  $0.05\nu_{\text{max}}$ , through the flare. When plotted against the flux at the lower frequency, the spectral index exhibits a characteristic loop-like pattern, which is tracked in the clockwise sense by the system. This type of pattern is well-known and has been observed at different wavelengths in several sources e.g., OJ 287 (Gear et al. 1986), PKS 2155–304 (Sembay et al. 1993) and Mkn 421 (Takahashi et al. 1996). It arises whenever the spectral slope is controlled by synchrotron cooling, (or, in fact, any cooling process which is faster at higher energy) so that information about changes in the injection propagates from high to low energies (Tashiro et al. 1995).

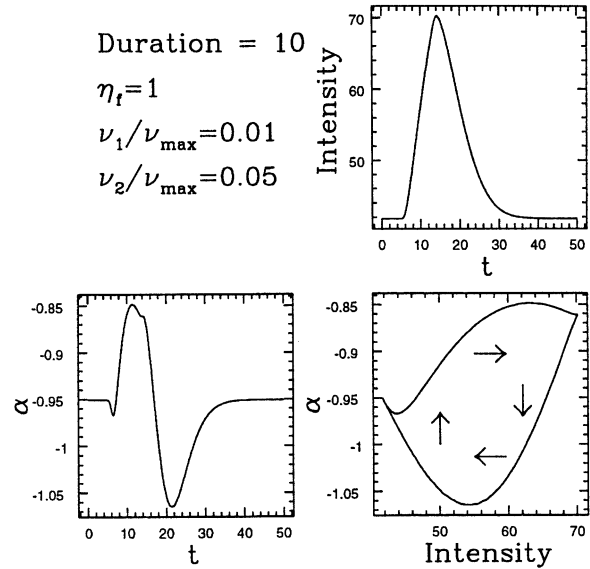


**Fig. 3.** The intensity and spectral index during the flare described by Eq. (23), as a function of time at low frequency. The loop in the  $\alpha$  vs. intensity plot is followed in the clockwise direction.

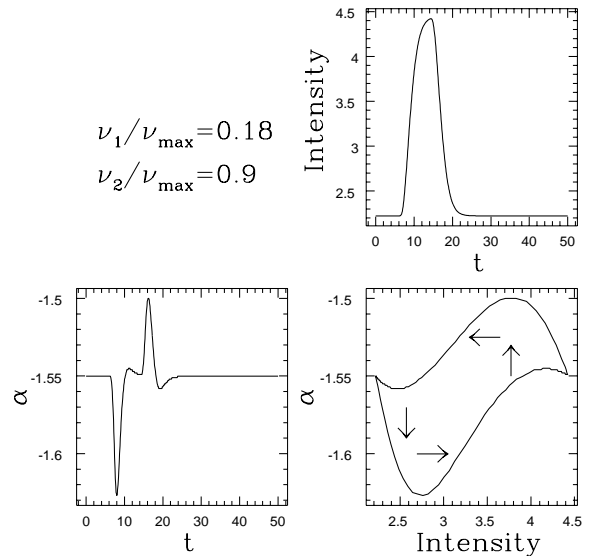


**Fig. 4.** The intensity and spectral index in the same flare as in Fig. 3 but at high frequency. The loop in the  $\alpha$  vs. intensity plot is followed in the anticlockwise direction.

If the system is observed closer to the maximum frequency, where the cooling and acceleration times are equal, the picture changes. Here information about the occurrence of a flare propagates from lower to higher energy, as particles are gradually accelerated into the radiating window. Such behaviour is depicted in Fig. 4, where the same flare is shown at frequencies which are an order of magnitude higher than in Fig. 3. In the case of Mkn 501, the frequency range is close to  $10^{18}$  Hz. This time the loop is traced anticlockwise. Such behaviour, although not as common, has also occasionally been observed, for example in the case of PKS 2155–304 (Sembay et al. 1993).

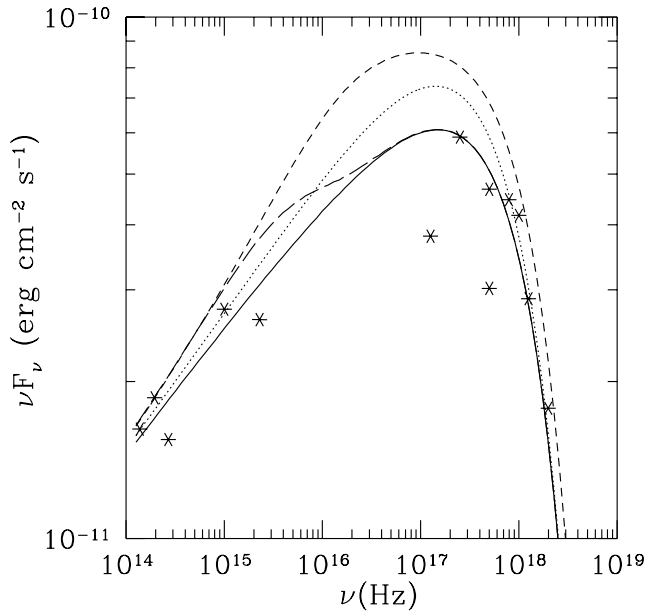


**Fig. 5.** The spectrum at times  $t = 0$  (solid line), 10 (dotted), 20 (short-dashed) and  $30t_{\text{acc}}$  (long-dashed) during the flare shown in Figs. 3 and 4. Data points are taken from Catanese et al. (1997).

Finally, in the region of the spectrum below the break, where the spectral index in the case of Mkn 501 is close to  $\alpha = -0.25$ , the emission is determined by the finite size of the source region, as expressed by  $t_b$ . Here, the flare shown in Figs. 3 and 4 has only a very small effect on the observed flux, since the duration  $t_f = 10t_{\text{acc}}$  has been chosen to be much smaller than the time  $t_b$  taken to fill up the emitting region with radiating particles. However, even in the case of a larger flare, or one of longer duration, no variation of the spectral index is to be expected through the flare at frequencies below the break, because the time taken to fill the effective emitting region is independent of frequency.

This effect of smaller changes in the spectral slope at lower frequencies is also evident from Fig. 5, where the spectrum is shown at times  $t = 0$  (i.e., the stationary emission as shown in Fig. 2),  $t = 10t_{\text{acc}}$ ,  $t = 20t_{\text{acc}}$ , and  $t = 30t_{\text{acc}}$ . Here it can be seen that the rise in emission is rapid at all frequencies, and the subsequent fall sets in as a wave which propagates downwards in frequency.

The results presented in Figs. 3 and 4 are computed for  $u_s = 1/10$ , so that the effects of the finite light travel time between the front and back of the source are negligible. In fact, in the limit  $u_s \rightarrow 0$ , Eqs. (7) to (24) reduce to the equations for a homogeneous source, provided the limit is taken keeping  $t_b$  finite, i.e., allowing the maximum spatial extent of the source  $u_s t_b$  to vanish.

#### 4. Discussion

It is generally accepted that the emission mechanism responsible for the radio to optical emission of blazars is the synchrotron process. In objects similar to Mkn 501, which is discussed in

Sect. 3, the synchrotron emission extends up to X-ray energies. It has recently emerged that a model in which the radiating relativistic electrons reside in a region of uniform magnetic field can provide a reasonable fit to observations not only of the synchrotron component, but also, via the inverse Compton scattering of the synchrotron photons, to gamma-ray observations in the GeV to TeV range. In this paper, we have introduced a detailed model of the emission region including the processes of acceleration and synchrotron cooling. This should ultimately help us to assess how accurately a homogeneous region can reproduce the observed synchrotron emission. In combination with a computation of the inverse Compton emission, the physical conditions and the geometry of the emission zone can be constrained.

The model used to describe acceleration is similar to that used by Ball & Kirk (1992) to describe the nonthermal radio emission of SN1987A. It involves a phenomenological division of the particle population into two groups: particles which are undergoing both acceleration and cooling and particles which merely cool. As a result, distributions are found which extend to a maximum value of the Lorentz factor, and then cut-off abruptly. The synchrotron emission from such a distribution fits well with that from the source we have discussed in Sect. 3 – Mkn 501. However, the form of the spectrum, especially in the hard X-ray region, depends on the shape of the cut-off of the electron spectrum. In our model, the sharpest possible turn-over is produced. Inhomogeneities within the source or refinements of the acceleration model result in a broader turn-over. This indicates that in the case of Mkn 501 a homogeneous model of the region in which synchrotron X-rays are emitted is a good approximation. It also confirms that a detailed model of the cut-off – which would necessarily involve additional parameters – is unnecessary. In other blazars e.g., Mkn 421 as well as in other synchrotron emitting objects e.g., SNR1006 (Mastichiadis & de Jager 1996), a broader cut-off is indicated by the observations. Our current computations suggest that if the physical situation is similar to that in Mkn 501, the broadening of the cut-off should be attributed to inhomogeneities within the source rather than an intrinsic property of the acceleration mechanism.

The variability predicted for a homogeneous source depends on the frequency of observation and the parameters of the acceleration mechanism – for relatively low frequency radiation, a characteristic pattern is produced, as pointed out by several groups. We have shown that closer to the maximum emitted frequency, this pattern should change. However, the observed variability depends not only on the intrinsic time-dependence, but also on the smoothing caused by light travel time delays across the source. We have described in detail the situation when the observer is positioned exactly on the axis of the source so that the emitting plasma moves directly towards the observer. This assumption is not as restrictive as it might at first sight appear, since the emission from a source in relativistic motion with Lorentz factor  $\Gamma$  is significantly boosted when viewed from a direction which makes an angle of less than  $\sim 1/\Gamma$  with the velocity. Intrinsic time variations within the source then appear shorter by a factor  $\Gamma$  (see Sect. 2). These are also smoothed out

on the timescale  $R/(c\Gamma)$ , where  $R$  is a typical dimension of the source perpendicular to the line of sight, provided that the angle between the source velocity and line of sight is of the order of  $1/\Gamma$ . It is a good approximation to neglect this smoothing if the intrinsic synchrotron cooling time, measured in the rest frame of the emitting plasma, is longer than the light travel time  $R/c$ . The same restriction applies to the size of the source along the direction to the observer. Here, however, the intrinsic variations always dominate if  $u_s \ll c$ . The general formulae given in Sect. 2 are valid also for relativistic  $u_s$ , but in the examples predicted, we have restricted ourselves to  $u_s = c/10$ . Whether or not intrinsic variability dominates over light travel time effects depends on the frequency of observation. For Mkn 501, for example, we have found that the maximum timescale over which particles cool is determined by the position of the spectral break and is roughly 700 times the synchrotron cooling time at the maximum emitted frequency. Thus, depending on  $R$ , there may exist a critical frequency above which variations are smoothed out by light travel time effects, but below which the results of Sect. 3 are valid. A detailed model of the inverse Compton emission is needed to estimate this frequency.

*Acknowledgements.* We acknowledge support for this work from the Deutsche Forschungsgemeinschaft under SFB 328 (A.M.) and DFG Ma 1545/2-1 (F.R.).

## Appendix A: energy dependent acceleration and escape

In general, one might expect the acceleration time  $t_{\text{acc}}$  and escape time  $t_{\text{esc}}$  introduced in Eq. (1) to be functions of particle energy. In this case the solution Eq. (3) is modified. Defining

$$f(\gamma) = \frac{\gamma}{t_{\text{acc}}(\gamma)} - \beta_s \gamma^2 \quad (\text{A1})$$

which is positive in the range of interest, one can write

$$\frac{\partial N}{\partial t} + \frac{\partial}{\partial \gamma} [f(\gamma)N] + \frac{N}{t_{\text{esc}}(\gamma)} = Q_0 \Theta(t) \delta(\gamma - \gamma_0) . \quad (\text{A2})$$

The solution of this equation subject to the boundary condition  $N(\gamma, 0) = 0$  is easily found using Laplace transforms:

$$N(\gamma, t) = \frac{Q_0}{f(\gamma)} \Theta[t - \tau(\gamma)] \exp \left[ - \int_{\gamma_0}^{\gamma} \frac{d\gamma'}{t_{\text{esc}}(\gamma') f(\gamma')} \right] \quad (\text{A3})$$

where

$$\tau(\gamma) = \int_{\gamma_0}^{\gamma} \frac{d\gamma'}{f(\gamma')} \quad (\text{A4})$$

In addition to the straightforward case  $t_{\text{acc}} = \text{constant}$ ,  $t_{\text{esc}} = \text{constant}$  dealt with above, it is also interesting to consider the case in which both of these quantities are linearly proportional

to  $\gamma$ . This would arise in modelling diffusive acceleration with a ‘gyro-Bohm’ spatial diffusion coefficient (e.g., Kirk et al. 1994). The solution is

$$N(\gamma, t) = \Theta[t - \tau(\gamma)] \frac{Q_0 t_{a,0} \gamma_{\text{max}}^2}{(\gamma_{\text{max}}^2 - \gamma^2)} \left[ \frac{\gamma(\gamma_{\text{max}}^2 - \gamma_0^2)}{\gamma_0(\gamma_{\text{max}}^2 - \gamma^2)} \right]^{-t_{a,0}/t_{e,0}} \quad (\text{A5})$$

with

$$\tau(\gamma) = \frac{t_{a,0}}{2} \log \left[ \frac{(\gamma_{\text{max}} + \gamma)(\gamma_{\text{max}} - \gamma_0)}{(\gamma_{\text{max}} - \gamma)(\gamma_{\text{max}} + \gamma_0)} \right] \quad (\text{A6})$$

and where we have written

$$t_{\text{acc}}(\gamma) = \gamma t_{a,0} \quad t_{\text{esc}}(\gamma) = \gamma t_{e,0} \quad (\text{A7})$$

Note that in this case the power-law index  $s$ , defined by  $N \propto \gamma^{-s+2}$  is related to the timescales by  $s = 2 + t_{a,0}/t_{e,0}$ , whereas in the case of energy independent acceleration and escape  $s = 3 + t_{\text{acc}}/t_{\text{esc}}$ .

## References

- Ball L.T., Kirk J.G., 1992 ApJ 396, L39  
 Bradbury S.M. et al. 1997 A&A 320, L5  
 Catanese M. et al. 1997 ApJ Letters 487, L143  
 Chiaberge M., Ghisellini G., 1997 in Proceedings of the Conference ‘From Micro to Mega Parsec’, second Italian conference on AGN, Memorie S.A.IT  
 Comastri A., Fossati G., Ghisellini G., Molendi S. 1997 ApJ 480, 534  
 Fritz K.D., Webb G.M. 1990 ApJ 360, 387  
 Gear W.K., Robson E.I., Brown L.M.J. 1986 Nature 324, 546  
 Inoue S., Takahara F. 1996 ApJ 463, 555  
 Kirk J.G., Heavens A.F. 1989 MNRAS 239, 995  
 Kirk J.G., Melrose D.B., Priest E.R. 1994 Plasma astrophysics, eds. A.O. Benz, T.J.-L. Courvoisier, Springer, Berlin  
 Maraschi L., Ghisellini G., Celotti A. 1992 ApJ 397, L5  
 Marscher A.P. 1980 Nature 288, 12  
 Marscher A.P., Gear W.K. 1985 ApJ 298, 114  
 Marscher A.P., Travis J.P. 1996 A&AS 120C, 537  
 Mastichiadis A., de Jager O.C. 1996 A&A 311, L5  
 Mastichiadis A., Kirk J.G., 1997 A&A, 320, 19  
 Meisenheimer K., Heavens A.F. 1987 MNRAS 225, 335  
 Melrose D.B. 1980 Plasma Astrophysics Vol I, Gordon & Breach, New York  
 Sikora M. 1994 ApJS 90, 923  
 Sembay S., Warwick R.S., Urry C.M., Sokoloski J., George I.M., Makino F., Ohashi T., Tashiro M. 1993 ApJ 404, 112  
 Takahashi T., Tashiro M., Madejski G., Kubo H., Kamae T., Kataoka J., Kii T., Makino F., Makishima K., Yamasaki N. 1996 ApJ 470, L89  
 Tashiro M., Makishima K., Ohashi T., Inada-Koide M., Yamashita A., Mihara T., Kohmura Y. 1995 PASJ, 47, 131